Faraday Discussions

Cite this: *Faraday Discuss.*, 2019, **215**, 379

Influence of carbonaceous species on aqueous photo-catalytic nitrogen fixation by titania†

Yu-Hsuan Liu,[a] Manh Hiep Vu,[b] JeongHoon Lim,[c] Trong-On Do [b] and Marta C. Hatzell [*c]

Received 19th November 2018, Accepted 5th February 2019
DOI: 10.1039/c8fd00191j

For decades, reports have suggested that photo-catalytic nitrogen fixation by titania in an aqueous environment is possible. Yet a consensus does not exist regarding how the reaction proceeds. Furthermore, the presence of an aqueous protonated solvent and the similarity between the redox potential for nitrogen and proton reduction suggest that ammonia production is unlikely. Here, we re-investigate photo-catalytic nitrogen fixation by titania in an aqueous environment through a series of photo-catalytic and electrocatalytic experiments. Photo-catalytic testing reveals that mineral phase and metal dopants play a marginal role in promoting nitrogen photofixation, with ammonia production increasing when the majority phase is rutile and with iron dopants. However, the presence of a trace amount of adsorbed carbonaceous species increased the rate of ammonia production by two times that observed without adsorbed carbon based species. This suggests that carbon species play a potential larger role in mediating the nitrogen fixation process over mineral phase and metal dopants. We also demonstrate an experimental approach aimed to detect low-level ammonia production from photo-catalysts using rotating ring disk electrode experiments conducted with and without illumination. Consistent with the photocatalysis, ammonia is only discernible at the ring with rutile phase titania, but not with mixed-phase titania. Rotating ring disk electrode experiments may also provide a new avenue to attain a higher degree of precision in detecting ammonia at low levels.

1 Introduction

Reports of photocatalytic nitrogen fixation on titania have surfaced for nearly eight decades.[1] Demonstrations have occurred in both the gas and aqueous

[a]*School of Civil and Environmental Engineering, Georgia Institute of Technology, Atlanta, Georgia 30313, USA*
[b]*Department of Chemical Engineering, Laval University, Rue de l'Université, Québec, QC G1V 0A6, Canada*
[c]*George W. Woodruff School of Mechanical Engineering, Georgia Institute of Technology, Atlanta, Georgia 30313, USA. E-mail: marta.hatzell@me.gatech.edu*

† Electronic supplementary information (ESI) available. See DOI: 10.1039/c8fd00191j

phase, and with various environmental conditions (relative humidity, temperature, pressure). Nearly all experimental observations suggest that abiotic nitrogen photofixation may be possible at ambient temperature and pressure.[2,3] This is impactful as it promotes the possibility for nutrient based fertilizer production from environmentally abundant materials (minerals) using only the sun as a source of energy.[33] Considering the state-of-the-art thermochemical approach to fertilizer production is responsible for consuming 1% of global energy and emitting 3% of global CO_2, photocatalytic nitrogen fixation could have a significant influence on improving the environmental impact associated with ammonia production.[2]

Photocatalytic nitrogen fixation also has environmental significance, as nitrogen fixation is a critical catalytic process in the nitrogen cycle. Although biological fixation is the most notable natural entry point for dinitrogen in soils, additional entry points driven through photon based reactions on earth abundant minerals are not outside the realm of possibility. A prominent Indian soil scientist (N. Dhar) in the 1940s suggested that the generation of fixed nitrogen in soils was possible through light based interactions.[1] Schrauzer and Guth explored this hypothesis further in the late 1970s through conducting a series of experiments aimed at discerning the photocatalytic nitrogen fixation activity on environmental catalysts (global sands).[3–5] This work concluded that the presence of titania in sands was responsible for nitrogen photofixation. Despite these intriguing findings, the potential impacts of photocatalytic nitrogen fixation on the nitrogen cycle is still limited to only back-of-the envelope based calculations.[6]

This slow progress is due to a lack of understanding regarding the catalytic processes that enable nitrogen fixation to occur on titania based photocatalysts. The wide band gap of the mineral coupled with the location of the band edges suggest that nitrogen reduction is unlikely. Furthermore, in environments were hydrogen evolution is possible (aqueous conditions), selectivity toward nitrogen reduction would require a low overpotential. Furthermore, the low measurable yields, high propensity for contamination and numerous sources of measurement error have all contributed to the significant debate regarding the probability of photocatalytic nitrogen fixation occurring on titanium dioxide.[7–11] Most prior studies have emphasized the role iron dopants and oxygen vacancies play in activating dinitrogen on titania.[12–14] Significant evidence supports the hypothesis that iron dopants aid in stabilizing oxygen vacancies, and that the presence of vacancies weakens the dinitrogen triple bond, enabling dinitrogen reduction. While possible, a more recent hypothesis suggests that carbon may play a critical role in nitrogen photofixation on titania.[15] Specifically, gas phase AP-XPS based experiments demonstrated that the presence of adventitious carbon was important for promoting interactions between titanium dioxide and nitrogen. The researchers hypothesized that a photocatalyzed carbon radical in concert with defects may promote nitrogen photofixation to ammonia. These gas phase experiments promote the need to understand if photocatalyzed carbon radicals also play a similar role in an aqueous photocatalytic environment.

Here, we aim to expand upon work completed in the gas phase; to explore the potential role carbonaceous species may play in promoting photo-catalytic nitrogen fixation in aqueous based experiments. While adventitious carbon and carbon dioxide may be the dominant carbonaceous species present in gas phase photocatalysis, here organic hole scavengers (methanol, ethanol and formic acid)

are the most prominent sources of carbon. We begin by probing the photocatalytic activity of rutile, mixed phase and iron-doped titania in the presence and absence of carbonaceous species. Rotating ring disk electrode experiments conducted on the catalyst also aim to determine if ammonia is detectable under illumination. Finally, the surface based active sites (oxygen vacancies and lattice iron) are mapped using bulk and surface based characterization.

2 Materials and methods

2.1 Catalysts preparation

A commercial rutile titanium dioxide and mixed phase titanium dioxide were purchased from US Research Nanomaterials Inc and Alfar Aesar (Haverhill, MA). Iron-doped titanium dioxide was prepared by standard sol–gel methods.[16] Titanium dioxide sols were prepared through the addition of 5 mL of titanium tetraisopropoxide (TTIP) solution into 50 mL of absolute ethanol. Then, the TTIP/ethanol solution was added (dropwise) into 50 mL of distilled water which was adjusted to pH 1.5 with chloric acid under vigorous stirring at room temperature. After continuously stirring for 24 h, the resulting transparent solution was evaporated using a rotary heater at 50 °C and dried in the oven at 70 °C overnight. The resulting particles were calcined at 500 °C for 1 h under air, and stored in air tight vessels. Catalyst cleaning prior to use occurred through a calcination process at 400 °C for 4 h. This cleaning procedure prevented the detection of any ammonia during controls, which were conducted in the absence of nitrogen (argon gas and light) and in the absence of light (nitrogen gas and dark).

2.2 Photocatalysis experiments

The photocatalytic nitrogen fixation experiments were conducted in a 500 mL reaction vessel at ambient temperature and atmospheric pressure. The temperature was fixed at 28 °C during the tests and was monitored to ensure a constant temperature existed under illumination. A 300 W Xenon–Mercury lamp (Newport Corporation – Irvine, CA) was used which contained a ultraviolet (UV) cutoff filter ($\lambda > 320$ nm) and an infrared (IR) cutoff filter. In all tests, 300 mg of photocatalyst was suspended in 300 mL of aqueous electrolyte. The aqueous electrolyte consisted of deionized water, or a mixture of deionized water with a hole scavenger. The hole scavenger concentration remained fixed at five volume percent. Methanol, ethanol and formic acid were chosen as representative hole scavengers. The photocatalytic reactor was deaerated using nitrogen gas (purity $\geq$ 99.999%) which was bubbled through this solution for thirty minutes in the dark. Various times were investigated to ensure that the solution was completely saturated with nitrogen and that all residual dissolved oxygen was removed. After saturation was reached, the reactor was irradiated with ultra-violet light ($\lambda > 320$ nm) from the top of the reactor. The reactor was continuously fed nitrogen gas during the entire twenty-four hour test period. Controls were conducted to probe the presence of contamination. In the first control, nitrogen gas was replaced by argon gas (purity $\geq$ 99.999%). All other conditions remained constant, including the degree of illumination. A second control was conducted in the dark with nitrogen gas. During all tests (including controls), approximately 5 mL of the suspension was removed from the reaction vessel at given intervals to test for ammonium.

2.3 Ammonium measurement

Two milliliters of dilute acid (0.005 M dilute H_2SO_4) was added to the catalyst suspension removed from the photocatalytic reactor. The dilute acid was used to promote ammonia desorption from the catalyst surface.[4] The particle suspension was then filtered by a 0.22 μm precision-glide syringe needle (Sigma-Aldrich, St. Louis, Mo) and syringe filters (Hach Co). The desorbed ammonium concentration was analyzed by ion chromatography using a cation exchange column (Aquion Dionex, Thermo Fisher). Ammonia was easily distinguished from other cations and had a retention time of 5.24 minutes. Standard solutions of ammonium chloride were used to create a calibration curve for the ion chromatograph. While many standard methods rely on optical measurements (UV-vis) whereby an organic compound reacts with ammonia (indophenol blue), we found these methods were susceptible to erroneous data, and a lack of reproducibility, consistent with prior works.[17]

2.4 Electrochemical characterization

Electrochemical testing was conducted using a rotating ring disk electrode experimental set up (Pine Research, Durham, NC). The catalyst was dispersed onto the disk, and the ring was poised to sense product (ammonia) formation. The catalyst was dispersed onto the disk using standard methods. A stock solution of 20% isopropanol and 0.5% Nafion solution was prepared by mixing 20 mL of isopropanol with 70 mL of distilled water and 10 mL of 5 wt% Nafion solution in a 100 mL volumetric flask. Then 25 mg of catalyst was added into the Nafion/IPA solution and sonicated for one hour. After the suspension was well dispersed without aggregation or sedimentation, 10 μL of the ink was drop cast onto the glassy carbon disk (6.2 mm diameter) and rotated at 1000 rpm for one hour using the air dry method.[18,19] A lamp (Asahi Spectra, Torrance, CA) was situated below the disk outside of the glass reactor. The lamp was used to irradiate the disk during experiments. A platinum ring (inner and outer diameter, 7 and 8.4 mm) served as the working electrode. A silver–silver chloride reference electrode (saturated potassium chloride) and a platinum wire counter electrode were also used. Cyclic voltammetry was performed while rotating the shaft of the working electrode at 500 rpm with a scan rate of 5 mV s^{-1}. Simultaneously, the ammonia oxidation reaction was investigated at the ring. In all testing the supporting electrolyte consisted of sodium hydroxide. Alkaline conditions were deemed necessary in order to promote the ammonia oxidation reaction.

2.5 Material surface characterization

The morphology of the titanium dioxide materials was investigated by scanning electron microscopy (SEM) coupled with an energy dispersive X-ray spectrometer (EDS). EDS coupled with XPS analysis confirmed that the iron-doped samples exhibited 0.69 atomic percent iron in the titania lattice. The as-prepared materials were identified through X-ray powder diffraction (XRD) using a Pananalytical Xpert Pro Alpha-1 XRD system for crystalline identification with Cu Kα radiation ($\lambda = 1.54051$). Step scanning was used with 2θ intervals from 10° to 90° with a residence time of 1 s. The chemical states of the surface elements were recorded using an X-ray photon spectrometer (XPS) using a Thermo K-Alpa XPS

spectrometer equipped with monochromatic Al Kα radiation as the X-ray source. The Ti2p, O1s, C1s, and Fe2p peaks were analyzed to access the surface properties (oxygen vacancies and dopants) of each catalyst.

3 Results and discussion

3.1 Photocatalytic testing with carbonaceous species

Photocatalysis in an aqueous phase reactor was conducted with the three catalysts. Two off the shelf titanium dioxide catalysts were chosen. The first off-the-shelf catalyst had a mineral composition that was primarily rutile phase. The second off-the-shelf catalyst had a mineral composition that was a mixture of anatase and rutile phases. A third catalyst was synthesized in the lab and contained iron dopants at 0.69 atomic percent, as confirmed through energy dispersive X-ray spectroscopy and XPS. Iron was chosen as the representative metal dopant, due to the demonstrated high activity reported in prior photocatalytic nitrogen fixation investigations.[4,14]

Photocatalytic experiments were conducted in three phases. In phase one, suspended particles were deaerated with either argon or nitrogen gas prior to illumination to remove all dissolved oxygen. The reactor was then illuminated for twenty-four hours, with samples removed at timed intervals. For all tests with argon, no ammonia was detected over the entire twenty four hour test. Dark controls in the presence of nitrogen also yielded no detectable ammonia. This confirmed that little nitrogen based contamination was present on the catalyst or photo-catalytic reactor prior to and during testing. Thus all ammonia detected was a result of a light-based reaction.

During the phase one experiments, the rate of ammonia production did not change regardless of the catalyst (rutile, mixed phase, and iron-doped titanium dioxide). The rate of ammonia production ranged from $0.25–0.38 \pm 0.03$ μM h^{-1} g^{-1}, indicating that the phase (rutile or anatase) and metal dopants (iron) did not play a significant role in improving the rate of nitrogen photofixation (Fig. 1 – phase 1). Prior investigations have highlighted that the phase (rutile)[4] and concentration of oxygen vacancies are critical material properties needed in order to increase the rate of ammonia production.[13] Furthermore, rutile phase catalysts have been shown both experimentally and theoretically to be active for both photo and electrocatalytic nitrogen fixation.[4,12]

Oxygen vacancies or point defects in the titanium dioxide lattice are also well known to exist in non-stoichiometric samples.[20] However, in the presence of oxygen or water, as is the case with aqueous-based photocatalytic experiments, vacancies can heal resulting in a near stoichiometric crystal. Thus, while oxygen vacancies may be active sites, the lifetime and concentration of these active sites are uncertain in a aqueous environment. We also note that the initial rates observed are in line with prior investigations, which contained catalysts with a low concentration of oxygen vacancies.[13]

After the initial phase, the minerals were separated and recycled back to the reactor for phase two. In phase two, a hole scavenger was introduced into the system. Traditional hole scavengers are organic compounds (*e.g.* EDTA, methanol and ethanol) which can be easily oxidized at the valance band by photogenerated holes (Fig. 1 – phase 2). Here, the aim in introducing a hole scavenger was not to minimize the rate of charge carrier recombination, but rather to probe the

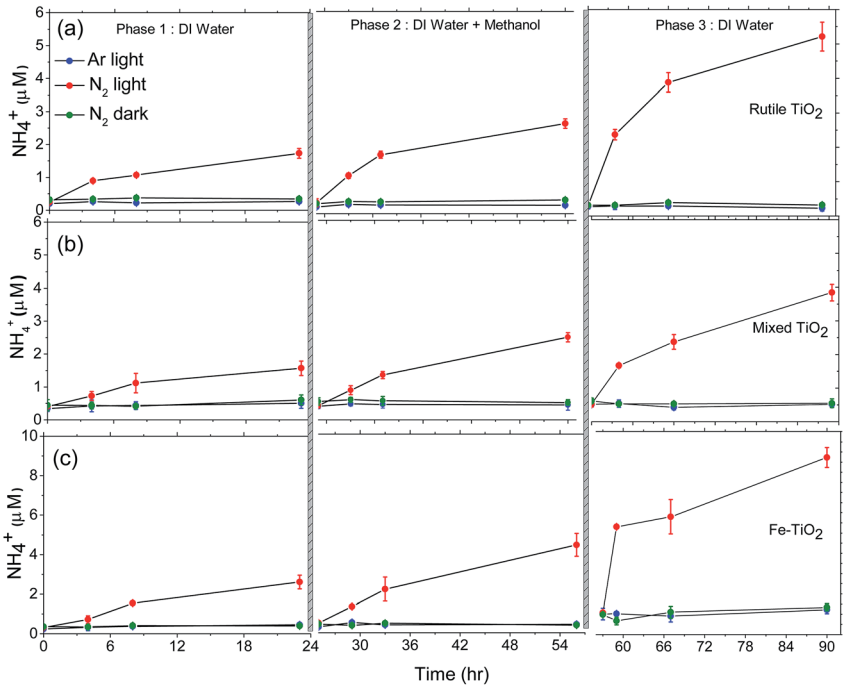

Fig. 1 Ammonia yield with time during photo-catalytic testing under a 300 W lamp. Experiments were conducted in three phases (labeled phase 1, 2 and 3 in figure), and with three catalyst (a) rutile titania, (b) mixed phase titania and (c) iron-doped titania.

hypothesis that nitrogen photofixation occurs due to an interaction with a photogenerated carbon radical. Methanol was chosen as a representative hole scavenger, as methanol is well studied with titania based photocatalytic systems, has been used as a hole scavenger in prior nitrogen fixation investigations, and has a well-documented reaction pathway.[21] Methanol oxidation is suspected to occur predominately through a dissociative pathway resulting in adsorbed methoxy species and hydroxyl groups.[22,23]

$$CH_3OH_{(a)} + O_{(a)} \rightarrow CH_3O_{(a)} + OH_{(a)} \quad (1)$$

The methoxy species have furthermore been shown to generate carbon-based radicals that have been detected through both infrared and electronic paramagnetic resonance based spectroscopy.[22] With this goal in mind, phase two proceeded with methanol present in the deionized water. Methanol was supplied to the deionized water at 5 vol%, which is consistent with the concentrations traditionally supplied to photocatalytic systems, whereby methanol acts as a hole scavengers. We will also note that in addition to the carbon radical generation due to the presence of methanol, a degree of adventitious carbon is also well known to exist on all titania based photocatalysts.

For each catalyst, the rate of ammonia production increased on average by 60% when compared to testing conducted without an organic hole scavenger, with the rates increasing to 0.4–0.65 $\pm$ 0.04 μM h^{-1} g^{-1}. This increase in the rate

of ammonia produced is traditionally ascribed to the system no longer being limited by the hole driven reaction (water splitting). Instead of oxidizing water, methanol is oxidized by the large oxidative potential of the holes generated in titanium dioxide, preventing charge carrier recombination. In phase two, the performance of rutile, mixed phase and iron-doped titania was similar, indicating that phase and metal dopants again did not alter performance significantly. In addition, controls (nitrogen dark and argon light) resulted in no appreciable ammonia production.

In an effort to probe the role of the carbon radical more directly, the catalysts were recycled a third time back in deionized water which contained no methanol. Here, by recycling the catalyst exposed to methanol oxidation, the aim was to remove the methanol, while maintaining a degree of adsorbed methoxy groups (or other oxidized carbon species) on the catalyst. Prior investigations have shown that methanol desorbs easily from the catalyst and solution at 308–373 K, while the methoxy groups remain adsorbed ($T_{des} = 460$ K).[23,24] Thus we hypothesize that in phase three, carbon radical generation may be possible in the absence of methanol due to these adsorbed species. In phase three, each catalyst experienced an increase in the rate of ammonia production (Fig. 1 – phase 3) over testing with methanol (phase two), and more importantly over results observed with just deionized water (phase one). In addition, the rate of ammonia production differed between the three individual catalysts. The rate of ammonia produced on the iron-doped titania, rutile titania and mixed phase titania were 1.3 ± 0.07 μM h^{-1} g^{-1}, 0.76 ± 0.06 μM h^{-1} g^{-1} and 0.56 ± 0.03 μM h^{-1} g^{-1}. Thus the order of photocatalytic activity for the three catalysts was iron-doped > rutile > mixed phase (Fig. 1). We also conducted control experiments (rutile titania) in which the catalysts were recycled three times without an organic scavenger. In these tests, that the ammonia yield remained at 0.2 ± 0.008 μM h^{-1} g^{-1} (consistent with the results obtained from phase 1), indicating that the increased rates are not a result of catalyst recycling and handling.

Phase three photocatalytic testing clearly emphasizes that the adsorbed carbon radicals most likely play a role in mediating the nitrogen fixation process on titania, as the performance increase cannot be ascribed to the presence of the hole scavenger. Additional testing also conducted with ethanol and formic acid resulted in similar trends (Fig. SI3†), with slight improvements observed with formic acid. Prior theoretical insight suggests that the carbon radicals have free energy (−1.89 eV) for nitrogen, which ultimately can aid in adsorbing and reacting dinitrogen.[12] Thus, the observed photocatalytic activity demonstrated here in an aqueous environment aligns with the prior gas phase experiments. With a range of reported values observed with photocatalytic nitrogen fixation based experiments on titania based photocatalysts,[4,7,13] here we highlight that in addition to material properties (bulk and surface), the carbon species prominently used within the photocatalytic reactor may also influence the nitrogen fixation reaction mechanism and catalytic activity.

3.2 Electrocatalytic characterization of titania

In addition to monitoring the ammonia production through bulk phase photocatalytic testing, we also probed the formation of ammonia through a series of rotating ring disk electrode (RRDE) experiments. The three catalysts (rutile, mixed

phase and iron-doped titanium dioxide) were investigated through dispersing the catalyst on the disk, while the ring was then poised at the ammonia oxidation potential. The aim of the ring is to act as a sensor to detect products formed as a result of the photocatalyzed reactions (hole and electron driven) on the titanium dioxide. The disk therefore was alternatively excited and not excited by light that was situated below the catalyst. The experiments were carried out with nitrogen and argon saturated electrolytes in the dark and light. A key difference between the photocatalytic experiments and the electrocatalytic experiments is the choice of electrolyte. While ideally, DI water would have been investigated, there were two chief challenges. The first being that ammonia oxidation in a highly resistive cell would produce very little current. With the goal being to correlate photocatalyzed ammonia production to ring current, we needed to limit resistance through the use of a supporting electrolyte. Another challenge was that ammonia oxidation occurs through the following proposed mechanism on Pt:

$$NH_3 + OH^- \rightarrow NH_{2,ad} + H_2O + e^- \quad (2)$$

$$NH_{2,ad} + OH^- \rightarrow NH_{ad} + H_2O + e^- \quad (3)$$

$$NH_{x,ad} + NH_{y,ad} \rightarrow N_2H_{x+y,ad} \quad (4)$$

$$N_2H_{x+y,ad} + OH^- \rightarrow N_2 + x + yH_2O + x + ye^- \quad (5)$$

Since the ring utilized here was Pt, in order to promote the ammonia oxidation reaction, OH^- is needed in the supporting electrolyte at significant concentrations. For this reason an alkaline electrolyte was chosen, as prior investigations have shown that ammonia oxidation on Pt cannot be detected in electrolytes with a pH lower than eight, and it is more preferable to operate with electrolytes that have a pH greater then ten.[25] It should be noted that titanium dioxide was not operated as an electrocatalyst, as titania was not electrochemically biased during the experiments.

In the control experiments, 0.1 M NH_4Cl was added to the supporting electrolyte and the ring voltage was swept from 0.2 *vs.* RHE to 1.2 *vs.* RHE. A noticeable peak was observed in all tests at $\approx$ 0.7 *vs.* RHE. This peak was attributed to ammonia oxidation and was used as a reference for future testing conducted with titanium dioxide (Fig. 2a).[26] Initial testing conducted with rutile titanium dioxide resulted in no peak during initial tests without light (Fig. 2b – 0 h). However, with the addition of light, the ammonia oxidation peak was observed. The catalyst was tested over a 10 hour period while illuminated, and the peak position did not vary significantly, while the peak current increased slightly. The extended experiment suggests that the rate of ammonia produced and oxidized remained constant with time (Fig. 2b – 5, 10 h). The other peaks besides ammonia oxidation are Pt–O formation (potential region 0.8–1 V), Pt–O reduction (potential region 1.2–0.7 V *vs.* RHE), Pt–H reduction (*ca.* 0.3 V *vs.* RHE) and Pt–H oxidation (*ca.* 0.35 V *vs.* RHE).

The three catalysts were first evaluated under similar conditions tested in the photocatalytic reactor. Namely, in an electrolyte saturated with nitrogen and argon gas, and under dark and light conditions. With the rutile phase titanium dioxide photocatalyst, the ammonia oxidation peak (*ca.* 0.7 V *vs.* RHE) was observed with nitrogen gas and light (Fig. 3a). No ammonia oxidation peak was present when

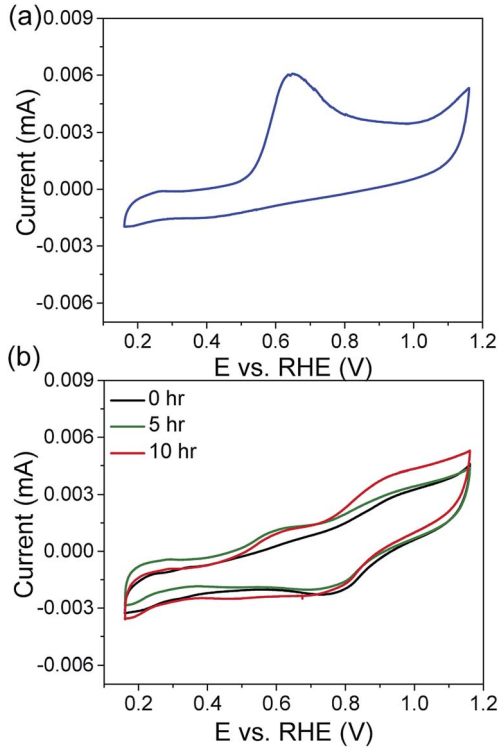

Fig. 2 (a) Ammonia oxidation peak observed on the Pt ring with 0.1 M NH_4Cl in the alkaline supporting electrolyte. (b) Ammonia oxidation of rutile TiO_2 under light and nitrogen gas.

nitrogen was replaced by argon, or when the sample was not illuminated (dark testing with nitrogen gas). In the potential region from 0.8–1.0 V *vs.* RHE, a Pt–O peak was observed. This is due to the presence of oxygen, being formed under oxidative potentials on Pt. Furthermore, when scanning negatively in the potential region from 1.2–0.7 V *vs.* RHE, Pt–O reduction occurred. A Pt–H desorption peak was observed in the potential region around 0.3 V *vs.* RHE under the negative scan and its redox couple was present around 0.35 V *vs.* RHE due to Pt–H oxidation.[18] These peaks were consistent for all catalysts, which is to be expected as the Pt based reactions are independent of the disk catalyst.

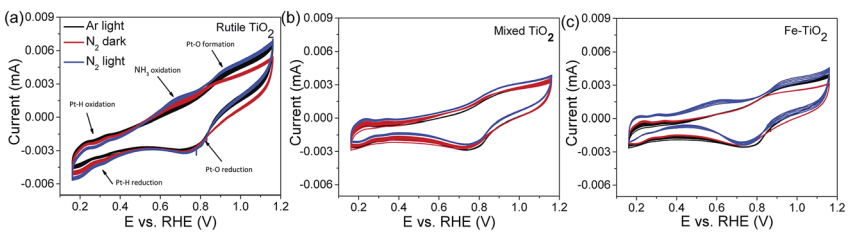

Fig. 3 Rotating ring disk electrode experiments with and without light in argon and nitrogen atmospheres with (a) rutile (b) mixed phase and (c) iron-doped titania.

When the mixed phase titanium dioxide was used as the catalyst, no ammonia oxidation peak was visible under nitrogen (light and dark) and argon (light). Prior investigations have suggested that a mixed phase photocatalyst is non-ideal for nitrogen fixation, as rutile may be the most active phase. Furthermore, mixed phase photocatalysts are most active for hydrogen evolution. Since hydrogen evolution competes with nitrogen reduction it is not surprising that ammonia was not detected with the mixed phased photocatalyst (Fig. 3b). With the iron-doped titania sample a more obvious ammonia oxidation peak was observed under nitrogen in the light. Again, controls with argon and nitrogen (dark) did not result in a peak (Fig. 3c). The observed peak currents (ammonia oxidation peaks) measured in the ring electrode were in-line with the photocatalytic testing activity, which suggests that rutile phase and iron-doped titania are active for nitrogen fixation, whereas the mixed phase photocatalyst is the least active catalyst. The current and the charge from the ammonia oxidation area can be used to estimate the rate of nitrogen photofixation. The observed rates for the rutile and iron-doped titanium dioxide were on the order of 10^{-6} mol per second, whereas the mixed phase catalyst was on the order of 10^{-8} mol per second. Furthermore, the cyclic voltammetry of the Pt disc electrode under nitrogen and argon gas flows, with and without light are shown in ESI Fig. SI1.† As shown, the Pt–O formation/reduction and Pt–H oxidation/reduction remained, but no ammonia oxidation was found with these three conditions indicating that Pt does not participate in ammonia formation with light illumination. Also, the most active iron-doped catalyst has been selected to perform the same phases 1–3 used during photocatalytic testing. The results were shown in Fig. SI2.† In phase one, iron-doped TiO_2 was examined under nitrogen flow and light. After phase one, the disk is recycled back in an electrolyte which contains methanol. In phase two methanol is oxidized when the disk is illuminated (presumably generating carbon radicals). The methanol oxidation peak was observed at 0.8 V *vs.* RHE. In phase 3, the electrolyte is replaced (no methanol), while adsorbed methoxy groups remain. The result showed that the residual adsorbed surface groups again increased the ammonia formation, observable through the increase in the peak area (*ca.* 0.7 V *vs.* RHE). The observed rate of ammonia oxidation in phase three is 2 times higher than that in phase one. Also, the CV showed that no adsorbed methanol remained on the surface of the catalyst since there is no methanol oxidation presented in the phase three experiment.

3.3 Catalyst surface and bulk characterization

Both the photocatalytic testing and rotating ring disk electrode experiments provide evidence that the rate of nitrogen photofixation is greatest on the iron-doped titanium dioxide, followed by the rutile phase catalyst and the mixed phase catalyst. Material characterization was obtained by X-ray photoelectron spectroscopy (XPS) and X-ray powder diffraction (XRD). XPS provided insight into the degree of oxygen vacancies that were present in the catalyst, and the degree of iron dopant at the surface of the catalyst. It should be noted that the *ex situ* analysis provides indirect evidence regarding the likelihood that a given catalyst has oxygen vacancies. It is not capable of determining how stable the vacancies are when immersed in the aqueous solution.

For the XPS, the Ti2p, O1s, C1s, and Fe2p regions were all analyzed. Determination of the degree of oxygen vacancies can be observed through monitoring the differences in the O1s and Ti2p regions (Fig. 4). The O1s spectra typically contains two sub-peaks, one which represents the lattice oxygen and a second which details the surface Ti_2O_3 groups. The Ti2p is typically fit with two peaks, $Ti2p_{3/2}$ and $Ti2p_{1/2}$ (Fig. 4b). In a well coordinated sample with no oxygen vacancies these peaks are sharp and are assigned to Ti^{4+} atoms. As the $Ti2p_{3/2}$ and $Ti2p_{1/2}$ broaden, two additional peaks can be introduced which are assigned to Ti^{3+} sites. Thus the two signatures of oxygen vacancies is the increase in Ti_2O_3 groups (Fig. 4a) and the increase in the concentration of Ti^{3+} sites. For the photocatalysts tested, we see that the most active samples have a higher degree of these two signatures, indicating that in the dry state, the amount of oxygen vacancies is indeed higher.[27,28]

According to the XPS analysis of Ti2p, we observed that the area of Ti^{4+} is 80% and Ti^{3+} is 20% in rutile TiO_2. Meanwhile, the area of Ti^{4+} is 86% and Ti^{3+} is 14% for iron-doped TiO_2. However, mixed TiO_2 consisted of 93% Ti^{4+} and 7% Ti^{3+}. Similarly in the O1s spectra, TiO_2 revealed 90% lattice oxygen and 10% Ti_2O_3. The iron-doped TiO_2 consisted of 91% lattice oxygen and 9% Ti_2O_3. The mixed TiO_2 has 97% lattice oxygen and 3% Ti_2O_3. The results reveal that both iron-doped and rutile TiO_2 have comparable oxygen vacancies or defects and mixed TiO_2 has the least. The iron dopant on the surface of TiO_2 plays a role as an electron carrier which will help create more Ti^{3+} and aid nitrogen adsorption onto the surface of

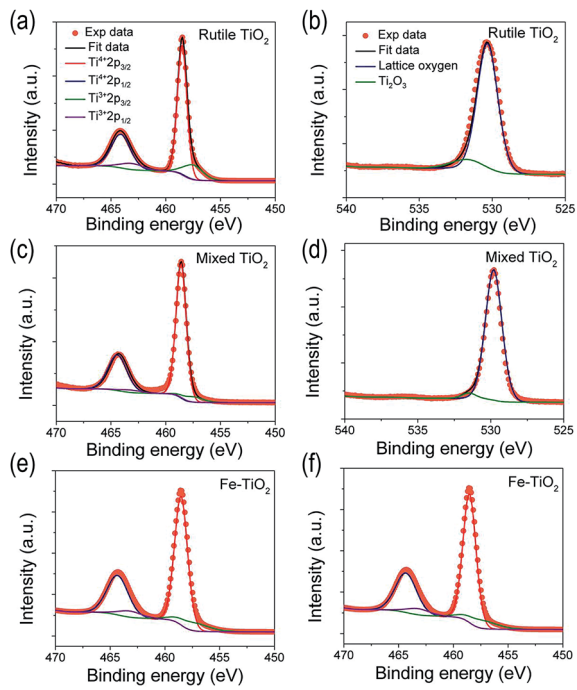

Fig. 4 XPS of rutile, mixed phase and iron-doped titanium dioxide samples. (a, c and e) Ti2p region and (b, d and f) O1s region of the XPS spectra for the three samples.

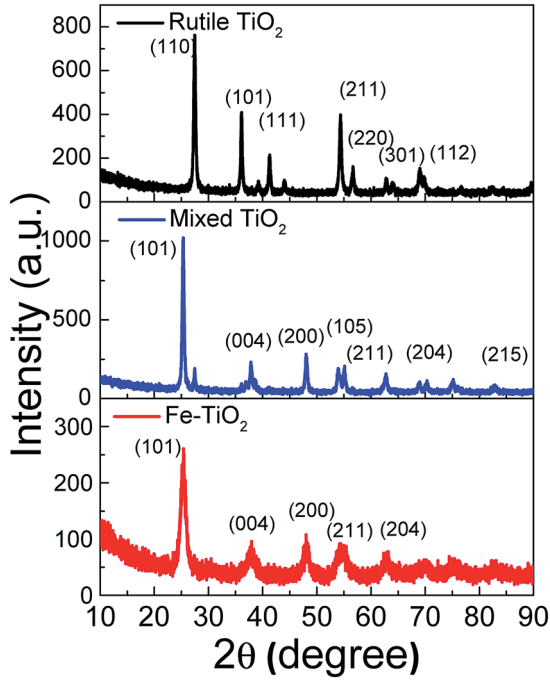

Fig. 5 XRD analysis of the rutile, mixed phase and Fe-doped titanium dioxide based photocatalysts.

TiO_2.[29,30] Therefore the results are consistent with the photocatalytic testing with iron-doped TiO_2 >rutile TiO_2 > mixed TiO_2.

In addition to the surface properties, XRD aided in identifying the structure of the three catalysts. All diffraction lines are relatively strong indicating a high crystallinity for all the samples. Furthermore, the peak positions and relative intensities of the diffraction lines match well with the standard diffraction data for different titanium dioxide phases (*i.e.* rutile and anatase). For rutile titanium oxide, the major peaks observed at 2θ values of 27.4°, 36.1°, 41.3°, 54.4°, 56.3°, 69.3° and 70.1° could be indexed to (110), (101), (111), (211), (220), (301) and (112) (Fig. 5). The pattern is consistent with the standard XRD data (JCPDS, no. 21-1276). The pattern of mixed titanium dioxide is consistent with the XRD standard data (JCPDS, no. 21-1272) which showed a strong anatase crystalline phase.[31,32] The XRD spectra of the synthesized iron-doped titanium dioxide revealed that the material was more likely to be anatase than rutile.

4 Conclusions

Photocatalytic nitrogen fixation on titanium dioxide has been heavily investigated for nearly eighty years due to the potential relevance toward achieving the long standing goal of clean ammonia synthesis. Nitrogen photofixation is also an intriguing entry point to the abiotic nitrogen cycle, yet has not been thoroughly investigated due to a lack of understanding regarding how the catalytic process occurs on this wide-band gap material. Here, we aimed to test an emerging

hypothesis which emphasizes that carbon species may play an integral role in catalyzing the dinitrogen adsorption and reduction to ammonia. Through a controlled experimental procedure whereby methanol is oxidized to produce adsorbed carbon radical based species, we show that the rate of ammonia produced can be increased by as much as two times that observed through testing without adsorbed carbonaceous species. This work extends previous work conducted in the gas phase, which also highlighted the potential role adventitious carbon plays in promoting gas-phase nitrogen fixation. We also investigate a method to detect ammonia at low levels using a rotating ring disk electrode experimental set up. The results show that a noticeable ammonia oxidation peak is observed on the rutile and iron-doped titanium dioxide samples, yet is not detected with the mixed phase titania. With many questions regarding the robust nature of low level ammonia measurements, the potential to use current rather than optical or chromatography based methods could improve the resolution of micromolar measurements which is important for both photo and electrochemical nitrogen fixation based studies.

Conflicts of interest

There are no conflicts to declare.

Acknowledgements

The researchers thank Georgia Tech start up funding for supporting this work, as well as the Georgia Tech TI:GER program. This material is based upon work supported by the National Science Foundation under Grant No. 1846611.

References

1 N. Dhar, E. Seshacharyulu and N. Biswas, *Proc. Natl. Acad. Sci., India*, 1941, **7**, 115–131.
2 A. J. Medford and M. C. Hatzell, *ACS Catal.*, 2017, 2624–2643.
3 G. N. Schrauzer, in *Photoreduction of Nitrogen on TiO_2 and TiO_2-Containing Minerals*, ed. L. Zang, Springer, London, 2011, pp. 601–623.
4 G. Schrauzer and T. Guth, *J. Am. Chem. Soc.*, 1977, **99**, 7189–7193.
5 G. N. Schrauzer, N. Strampach, L. N. Hui, M. R. Palmer and J. Salehi, *Proc. Natl. Acad. Sci. U. S. A.*, 1983, **80**, 3873–3876.
6 T. A. Doane, *ACS Earth Space Chem.*, 2017, **7**, 411–421.
7 J. G. Edwards, J. A. Davies, D. L. Boucher and A. Mennad, *Angew. Chem., Int. Ed.*, 1992, **31**, 480–482.
8 D. L. Boucher, J. A. Davies, J. G. Edwards and A. Mennad, *J. Photochem. Photobiol., A*, 1995, **88**, 53–64.
9 G. Richardson, J. Davies and J. Edwards, *Fresenius' J. Anal. Chem.*, 1991, **340**, 392–394.
10 L. F. Greenlee, J. N. Renner and S. L. Foster, *The Use of Controls for Consistent and Accurate Measurements of Electrocatalytic Ammonia Synthesis from Dinitrogen*, 2018.
11 Y. Song, D. Johnson, R. Peng, D. K. Hensley, P. V. Bonnesen, L. Liang, J. Huang, F. Yang, F. Zhang, R. Qiao, *et al.*, *Sci. Adv.*, 2018, **4**, e1700336.

12 B. M. Comer and A. J. Medford, *ACS Sustainable Chem. Eng.*, 2018, **6**, 4648–4660.
13 H. Hirakawa, M. Hashimoto, Y. Shiraishi and T. Hirai, *J. Am. Chem. Soc.*, 2017, **139**, 10929–10936.
14 J. Soria, J. C. Conesa, V. Augugliaro, L. Palmisano, M. Schiavello and A. Sclafani, *J. Phys. Chem.*, 1991, **95**, 274–282.
15 B. M. Comer, Y.-H. Liu, M. B. Dixit, K. Hatzell, Y. Ye, E. J. Crumlin, M. C. Hatzell and A. J. Medford, *J. Am. Chem. Soc.*, 2018, **45**, 15157–15160.
16 J. Choi, H. Park and M. R. Hoffmann, *J. Phys. Chem. C*, 2009, **114**, 783–792.
17 X. Gao, Y. Wen, D. Qu, L. An, S. Luan, W. Jiang, X. Zong, X. Liu and Z. Sun, *ACS Sustainable Chem. Eng.*, 2018, **6**, 5342–5348.
18 Y. Garsany, O. A. Baturina, K. E. Swider-Lyons and S. S. Kocha, *Experimental methods for quantifying the activity of platinum electrocatalysts for the oxygen reduction reaction*, 2010.
19 B. Su, Y. Ma, Y. Du and C. Wang, *Electrochem. Commun.*, 2009, **11**, 1154–1157.
20 S. Wendt, R. Schaub, J. Matthiesen, E. K. Vestergaard, E. Wahlström, M. D. Rasmussen, P. Thostrup, L. Molina, E. Lægsgaard, I. Stensgaard, *et al.*, *Surf. Sci.*, 2005, **598**, 226–245.
21 D. A. Panayotov, S. P. Burrows and J. R. Morris, *J. Phys. Chem. C*, 2012, **116**, 6623–6635.
22 D. C. Hurum, A. G. Agrios, K. A. Gray, T. Rajh and M. C. Thurnauer, *J. Phys. Chem. B*, 2003, **107**, 4545–4549.
23 M. Shen and M. A. Henderson, *J. Phys. Chem. Lett.*, 2011, **2**, 2707–2710.
24 Q. Yuan, Z. Wu, Y. Jin, L. Xu, F. Xiong, Y. Ma and W. Huang, *J. Am. Chem. Soc.*, 2013, **135**, 5212–5219.
25 A. Kapałka, S. Fierro, Z. Frontistis, A. Katsaounis, S. Neodo, O. Frey, N. De Rooij, K. M. Udert and C. Comninellis, *Electrochim. Acta*, 2011, **56**, 1361–1365.
26 K. Endo, Y. Katayama and T. Miura, *Electrochim. Acta*, 2005, **50**, 2181–2185.
27 B. Bharti, S. Kumar, H.-N. Lee and R. Kumar, *Sci. Rep.*, 2016, **6**, 32355.
28 M. J. Jackman, A. G. Thomas and C. Muryn, *J. Phys. Chem. C*, 2015, **119**, 13682–13690.
29 R. Grau-Crespo and U. Schwingenschlögl, *J. Phys.: Condens. Matter*, 2011, **23**, 334216.
30 X. Pan, M.-Q. Yang, X. Fu, N. Zhang and Y.-J. Xu, *Nanoscale*, 2013, **5**, 3601–3614.
31 Y. Wang, L. Li, X. Huang, Q. Li and G. Li, *RSC Adv.*, 2015, **5**, 34302–34313.
32 J. Wang, J. Yu, X. Zhu and X. Z. Kong, *Nanoscale Res. Lett.*, 2012, **7**, 646.
33 B. M. Comer, P. Fuentes, C. O. Dimkpa, Y. Liu, C. A. Fernandez, P. Arora, M. Realff, U. Singh, M. C. Hatzell and A. J. Medford, *Joule*, 2019, **3**, 1–28.

